Biomaterials Advances 154 (2023) 213587

Contents lists available at ScienceDirect

Biomaterials Advances

journal homepage: www.journals.elsevier.com/materials-science-and-engineering-c

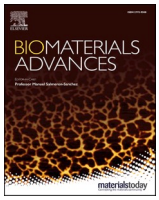

Bioinspired mineralization of engineered living materials to promote osteogenic differentiation

Belén Parra-Torrejón [a], Vineetha Jayawarna [b], Aleixandre Rodrigo-Navarro [b], Juan Gonzalez-Valdivieso [b], Oana Dobre [b], Gloria B. Ramírez-Rodríguez [a], Manuel Salmeron-Sanchez [b,*], José M. Delgado-López [a,*]

[a] Department of Inorganic Chemistry, University of Granada, Faculty of Science, Av. Fuente Nueva, s/n, 18071 Granada, Spain
[b] Centre for the Cellular Microenvironment, Mazumdar-Shaw Advanced Research Centre, University of Glasgow, Glasgow G11 6EW, UK

ARTICLE INFO

Keywords:
Living materials
Engineered bacteria
Calcium phosphate
Biomineralization
Osteogenesis
Tissue engineering

ABSTRACT

In this work, Engineered Living Materials (ELMs), based on the combination of genetically-modified bacteria and mineral-reinforced organic matrices, and endowed with self-healing or regenerative properties and adaptation to specific biological environments were developed. Concretely, we produced ELMs combining human mesenchymal stem cells (hMSCs) and *Lactococcus lactis (L. lactis)*, which was specifically programmed to deliver bone morphogenetic protein (BMP-2) upon external stimulation using nisin, into mineralized alginate matrices. The hybrid organic/inorganic matrix was built through a protocol, inspired by bone mineralization, in which alginate (Alg) assembly and apatite (HA) mineralization occurred simultaneously driven by calcium ions. Chemical composition, structure and reologhical properties of the hybrid 3D matrices were dedicately optimized prior the incorportation of the living entities. Then, the same protocol was reproduced in the presence of hMSC and engineered *L. lactis* that secrete BMP-2 resulting in 3D hybrid living hydrogels. hMSC viability and osteogenic differentiation in the absence and presence of the bacteria were evaluated by live/dead and quantitative real-time polymerase chain reaction (qPCR) and immunofluorescence assays, respectively. Results demonstrate that these 3D engineered living material support osteogenic differentiation of hMSCs due to the synergistic effect between HA and the growth factors BMP-2 delivered by *L. lactis*.

1. Introduction

Large bone defects due to traumatic injury, degenerative diseases, surgical removal of tumours or congenital diseases are still a major challenge in common clinical practice, being bone the second most transplanted tissue after blood [1,2]. The great demand for bone implants, exacerbated by an ageing population, has prompted the development of innovative materials able to foster the regeneration of damaged tissues [1,2]. The growing field of Engineered Living Materials (ELMs), which contain programmed living cells with responsive functions embedded in inert polymeric matrices, aims at recreating the ability of natural living materials (*e.g.*, bone, wood or bacterial biofilms) to adapt their composition, structure and performance in response to environmental cues [3]. To achieve this goal, living cells form or assemble the material itself through a bottom-up approach, or modulate the functionality of the material in some manner (top-down approach) [4]. Among the living entities, engineered bacteria, the most genetically tractable organisms, are of special interest to design programmable ELMs [4]. In fact, a breakthrough study in bone tissue engineering involved the control of human mesenchymal stem cell (hMSC) fate through engineered *Lactococcus lactis* (*L. lactis*), a Generally Recognized as Safe (GRAS) species of bacteria [5]. *L. lactis* was genetically modified to express a fragment encompassing the 7th–10th type III domains ($III_{7–10}$) of the human fibronectin (FNIII 7–10) providing a platform to support hMSCs adhesion, as well as expressing bone morphogenetic protein 2 (BMP-2) that induces osteogenic differentiation of hMSCs [5]. The growth factor-eluting engineered biofilm can continuously produce the desired dose of a therapeutic agent at the regeneration site to stimulate stem cell differentiation and bone tissue regeneration [5].

Despite these interesting features associated to programmable bacteria, most of them are vulnerable to harsh external environments, and can only survive or maintain their metabolic activity in relatively mild

* Corresponding authors.
E-mail addresses: Manuel.Salmeron-Sanchez@glasgow.ac.uk (M. Salmeron-Sanchez), jmdl@ugr.es (J.M. Delgado-López).

https://doi.org/10.1016/j.bioadv.2023.213587
Received 5 May 2023; Received in revised form 31 July 2023; Accepted 12 August 2023
Available online 14 August 2023

conditions [6]. Thereby, the incorporation of engineered bacteria into hydrogels (living hydrogels) is a robust strategy to protect the living entity and enhance their biological activity [7]. In addition, the resulting living hydrogels provide spatiotemporal control of the concentration of the chemicals released by the bacteria and reduce toxicity to normal tissues [7]. Biocompatible hydrogels, provide sufficient space to accommodate the genetically engineered bacteria and protect them against environmental damage, including antibiotics and acidic pH, increasing their lifespan and facilitating their retrieval [7]. Besides, hydrogels present tuneable physicochemical properties that allow the controlled release of therapeutic agents, increasing the efficacy of the bacteria-based therapy [7]. In fact, ELMs based on the encapsulation of engineered microorganisms in hydrogels have been developed for digestive health treatment, skin fungal infections, wound healing, living bacterial vaccines, and cancer bacteriotherapy [7–10].

Alginate is one of the most used polymers for cell encapsulation and alginate hydrogels are among the most employed materials for bone tissue engineering (BTE), bioprinting, drug delivery and antimicrobial and wound dressing applications [11,12]. This is due to their compositional and structural similarities to natural ECM and properties such as gelling capacity, high biocompatibility, low immunogenicity, and low cost [7,11,12]. In addition, alginate has been declared safe by the Food and Drug Administration (FDA) for several biomedical applications and in pharmaceutical industries [11,13]. Regarding BTE, the *in situ* gelation of alginate hydrogels by ionic crosslinking with divalent cations has been explored to encapsulate cells and growth factors in order to enhance bone healing process through the controlled delivery of cells and bioactive molecules [12,14]. Owing to the shear thinning character, rapid cross-linking ability and feasibility of printing viable cells, injectable alginate bioinks are also one of the most used biomaterials for bioprinting towards the development of scaffolds with a complex, patient specific external geometry in combination with a precise control over the internal architecture [12,14]. A recent study developed a prototype of a low-cost 3D bioprinting platform able to simultaneously encapsulate stem cells and genetically modified non-pathogenic bacteria (*Lactococcus lactis*) to induce osteogenic differentiation of human bone marrow–derived mesenchymal stem cells [15].

Despite the recent advances in ELMs, living hydrogels face still important challenges in bone regeneration to develop systems that recapitulate the properties of the natural bone ECM [16]. Bone is a complex hierarchical tissue mainly composed of a mineral phase, hydroxyapatite nanoparticles (HA, $Ca_{10}(PO_4)_6(OH)_2$), that grow preferentially aligned with the *c*-axis parallel to the longitudinal axis of the collagen fibres resulting in a hybrid biomaterial with unique biomechanical performance [17–19]. Bone mineralization has inspired the design of sophisticated materials with highly controllable and specialized properties for bone tissue engineering [20,21]. The gradual mixing of solutions containing an organic polymer and phosphate ions with solutions containing calcium ions enables the assembly of the polymer into 3D matrices (driven by either the pH increase or Ca-mediated polymer crosslinking) and simultaneously, the precipitation of apatite nanocrystals, governed by the organic matrix and ionic concentration of the precursors [20,22–24]. These bioinspired routes provide hybrid biomaterials, with composition and structure at the nanoscale similar to bone, and thus with enhanced bioactivity, osteoconductivity and osteoinductive, of special interest for bone tissue regeneration [12,25,26]. The integration of biomimetic HA nanoparticles into polymeric hydrogels results in hybrid materials, which rebuild the osteogenic micro-environment, capable to promote bone mineralization, construction of immune micro-environment, and favour angiogenesis both *in vitro* and *in vivo* [27]. 3D printing combined with *in situ* apatite mineralization has been also proposed as a potential strategy for bone tissue engineering [25]. However, this technology still needs improvement to produce biomaterials recapitulating osteogenic microenvironments. Other interesting strategy is combining bioceramic materials (HA and calcium sulphate) and BMP-2 into 3D scaffolds [28]. These composite materials (gelatin/bioceramic) allowed the sustained release of BMP-2, favouring the osteogenic differentiation of human bone-marrow derived mesenchymal stem cells (hBM-MSCs) and promoting bone regeneration in an osteoporotic defect model [28]. Despite the advances in the synergistic integration of therapeutically active growth factors and bioinspired HA mineral for bone regeneration therapy, avoiding supraphysiological BMP-2 doses and reducing consequently the possible adverse effects is still a challenge.

In this work, ELMs were synthesized by a bottom-up approach inspired in bone mineralization. We designed a method to produce the simultaneous alginate gelification and apatite mineralization in the presence of hMSC and engineered *L. lactis* bacteria resulting in 3D hybrid living hydrogels. Since alginate rapidly forms physically crosslinked gels when interacting with calcium ions, both processes (gelification and mineralization) are interconnected, enhancing the interactions and interplay between the organic/inorganic phases and favouring the formation of homogeneous hybrid hydrogels, in which the mineral is integrated in the organic matrix. The chemical composition, structure and mechanical properties of mineralized hydrogels were investigated. We show hMSC osteogenic differentiation only in the presence of the engineered bacteria demonstrating the synergistic potential of *L. lactis* bacteria expressing BMP-2 and biomimetic apatite mineral phase to direct stem cell fate.

2. Materials and methods

2.1. Synthesis of hybrid hydrogels

Alginate (Alg) hydrogels have been mineralized through a protocol emulating bone biomineralization in which Alg gelation and apatite (HA) mineralization occurred simultaneously producing 3D mineralized gels (Alg/HA, Fig. 1) [24,29]. A solution containing 1.5 mL of Na_2HPO_4 (0.12 M), 1.5 mL of $Na_3C_6H_5O_7$ (0.1 M), and 1.5 mL of Na_2CO_3 (0.1 M), was adjusted to pH 7.4 with HCl (5 M) in a 10 mL vial. After that, 101 mg of sodium alginate was added and mixed vigorously with vortex to obtain as-called alginate solution (Fig. 1). Finally, the addition of 2.25 mL of a calcium chloride solution (0.06–0.27 M) triggered the rapid formation of an Alg hydrogel due to ionic crosslinking with Ca^{2+} ions and the simultaneous mineralization of the polymer (Fig. 1). Several Ca^{2+} ion concentrations and thus, Ca/P molar ratio (above and below the stoichiometric value of hydroxyapatite, $Ca/P = 1.67$) were evaluated to optimize the mineralization of Alg hydrogels (Table 1). Control Alg hydrogels were synthesized through the same approach but using 1.5 mL of water instead of 1.5 mL of Na_2HPO_4 (0.12 M) to avoid HA mineralization. The hydrogels were incubated at 37 °C for 24 h and then, the consistency of the hydrogels was assessed by using the visual inverted vial method. Then, the hydrogels were repeatedly washed with ultrapure water by centrifugation (8000 rpm, 10 min, 18 °C) and freeze-dried (Telstar Cryodos freeze-drier) for further characterization. All reagents were purchased from Sigma Aldrich UK.

2.2. Physicochemical characterization

2.2.1. X-ray powder diffraction (XRPD)

XRPD data were collected on a Bruker D8 Discover diffractometer (from the Centre for Scientific Instrumentation of the University of Granada, CIC-UGR) using Cu Kα radiation ($\lambda = 1.5406$ Å) from 5° to 55° (2θ) with a scan rate of 40 s per step and a step size of 0.02° with a HV generator set at 50 kV and 1 mA.

2.2.2. Fourier transform infrared (FTIR)

FTIR spectra of freeze-dried hydrogels were recorded on a Tensor 27 (Bruker, Karlsruhe, Germany) spectrometer. 2 mg of the powder samples was mixed with 200 mg of anhydrous potassium bromide (KBr) and pressed at 5 tons into a 12 mm diameter disc using a hydraulic press (Specac). Samples were produced by triplicates and a pure KBr disk was

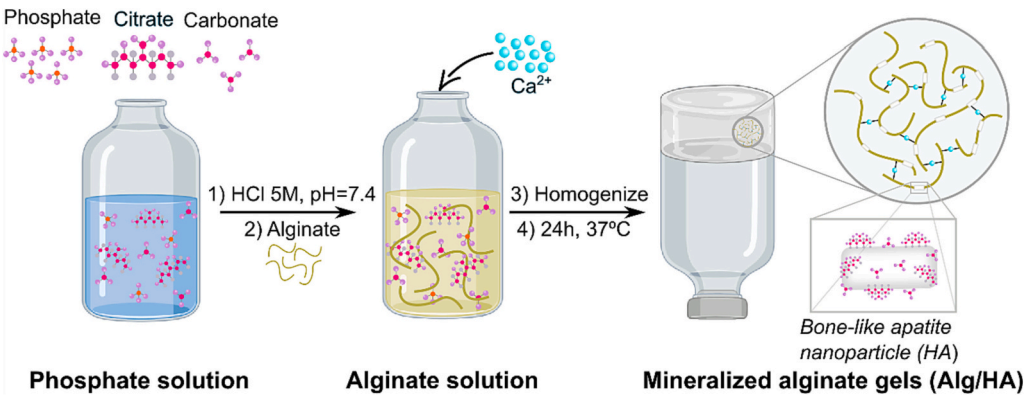

Fig. 1. Scheme of the preparation of mineralized alginate (Alg/HA) hydrogels. Firstly, a phosphate solution containing citrate and carbonate, two relevant components of bone apatite [30–32], is prepared. The pH of this solution is adjusted to 7.4 with concentrated hydrochloric acid solution before adding the sodium alginate solution. Then, the calcium solution is added and homogenized by vigorous vortexing to trigger alginate hydrogel formation and polymer mineralization at the same time. After 24 h at 37 °C, inverted vials reveal the consistence of the mineralized alginate hydrogels in each condition mentioned in Table 1.

Table 1
Final concentrations of alginate and ionic precursors for each mineralization experiment.

Alginate (%wt)	$Na_3C_6H_5O_7$ (mM)	Na_2CO_3 (mM)	Na_2HPO_4 (mM)	$CaCl_2$ (mM)	Ca/P ratio
1.5	22	22	27	13	0.5
1.5	22	22	27	29	1.08
1.5	22	22	27	36	1.33
1.5	22	22	27	40	1.67
1.5	22	22	27	60	2.23

used as a blank. The infrared spectra were recorded by accumulating 40 scans covering from 400 cm^{-1} to 4000 cm^{-1} at a resolution of 4 cm^{-1}.

2.2.3. Transmission electron microscopy (TEM)

TEM, Selected Area Electron diffraction (SAED) and High-Angle Annular Dark Field-scanning transmission electron microscopy (HAADF-STEM) images and Energy-Dispersive X-ray Spectroscopy (EDS) elemental maps were acquired with STEM FEI TALOS F200X microscope equipped with a 4 Super-X SDDs (Thermo Fisher Scientific Waltham, MA, USA) from CIC-UGR. For TEM analysis, hydrogels were washed vigorously with Milli-Q water and then, a 200-mesh copper grid covered with thin amorphous carbon films was immersed into the hydrogel. After 1 min incubation, the grids were washed carefully with ultrapure water five times (drops of 20 μL) and left to air-dry in ambient conditions.

2.2.4. Rheological characterization of the hydrogels

Mechanical characterization was performed using a torsional rheometer (MCR 302, Anton Paar, Austria) at a constant temperature of 25 ± 0.1 °C. Frequency sweep was first performed to evaluate the regime where the storage modulus (G') was independent of frequency (ω). Then, shear-strain sweep tests were set at 0.1 N, as normal force, using a plate-plate geometry of 8 mm diameter. Values of storage moduli (G') and loss moduli (G") at constant angular frequency (10 rad s^{-1}) were obtained within the linear viscoelastic regime (LVE) as a function of increasing strain sweep (γ) from 0.1 % to 1 %. In this regime, G' was independent of frequency and strain so that the shear modulus (G) of the hydrogels could be determined attending to $G=\lim_{\omega\to 0} G'(\omega)$ [33]. Results were reported as stiffness (Young's modulus, *E*) calculated *via* the Eq. (1), where *G* is the shear modulus and ν is referred to Poisson's ratio (assumed to be 0.5 for incompressible material) [34]:

$$E\ (kPa) = 2G(1+\nu) \quad (1)$$

The mechanical properties of mineralized (Alg/HA) and non-mineralized (Alg, control) hydrogels at different Ca^{+2} concentrations ($[Ca^{2+}]$ = 40 mM and $[Ca^{2+}]$ = 60 mM), incubated at 37 °C for 24 h were evaluated. Experiments were performed for each condition at least with 5 different samples. The samples were kept immersed in 1-phosphate-buffered saline (PBS) before testing to avoid water loss.

2.3. Cell and bacteria encapsulation

2.3.1. hMSC culture

Human bone marrow-derived mesenchymal stem cells (hMSCs) (PromoCell GmbH, Germany) were expanded and maintained in Dulbecco's modified Eagle's medium (DMEM) supplemented with 10 % fetal bovine serum (FBS), 1 % non-essential amino acids (NEAA), 1 % sodium pyruvate and 2 % antibiotics (6.74 U mL^{-1} penicillin-streptomycin, 0.2 μg mL^{-1} fungizone) and 2 mM L-glutamine, at 37 °C, in a humidified atmosphere with 5 % CO_2. Culture medium was replaced every 3 days. When 90 % confluency was reached, cells were washed with PBS and detached from the culture flask by using trypsin–EDTA. The cells were centrifuged at 1400 rpm for 5 min and then, resuspended in DMEM before proceeding with the cell culture. Expanded hMSCs were used at passages 2–3.

2.3.2. Bacterium culture

Engineered *L. lactis* NZ9020 [35] expressing the mature form of human BMP-2 secreted in the medium, under a nisin-inducible promoter, were grown in M17 medium supplemented with 0.5 % glucose and 10 μg mL^{-1} chloramphenicol. The M17 medium is composed of soya-peptone (5 g L^{-1}), "Lab-lemco" (5 g L^{-1}), tryptone (5 g L^{-1}), ascorbic acid (0.5 g L^{-1}), yeast extract (2.5 g L^{-1}), $MgSO_4$ (250 mg L^{-1}), and di-sodium glycerophosphate (19 g L^{-1}). The engineered bacteria were grown at 30 °C in static anaerobic conditions [5,36].

2.3.3. Fabrication of polydimethysiloxane moulds

Polydimethylsiloxane (PDMS) moulds were fabricated by mixing prepolymer silicone elastomer base solution and curing agent (Sylgard 184; Dow Corning Corporation) in a 10:1 ratio [37]. The mixture was homogenized, poured on a 140 mm Petri dish and degassed for 10 min in a vacuum chamber to remove bubbles. After that, the mixture was placed in an oven at 70 °C for 2 h. After crosslinking and cooling down, the polymer was cut to make moulds large enough to fit into a well from a 6-well plate and to include three holes with 6 mm diameter and 2 mm wide (200 μL capacity) where the hydrogels can be cast.

2.3.4. Cell encapsulation within mineralized alginate hydrogels

L. lactis and hMSCs were encapsulated in mineralized Alg hydrogels by adapting the protocol previously described in Section 2.1 for a Ca/P molar ratio of 1.67 (Table 1). hMSCs were suspended in 300 μL of the Alg solution containing Alg, phosphate, citrate, and carbonate, to a final concentration of 4.2 x 10^5 cells mL^{-1}. Then, 60 μL from a suspension of bacteria (1.15 x 10^7 CFU mL^{-1} in PBS) were added and homogenized. After that, 100 μL of this Alg solution was added to each hole in the PDMS moulds placed in a 6-well plate. To carry out the simultaneous Alg

hydrogel formation and mineralization in the presence of hMSCs and *L. lactis*, 50 μL of a calcium chloride 0.2 M solution was added to each hole to ensure the *in situ* entrapment of hMSCs and *L. lactis* within the 3D mineralized hydrogels (Alg/HA + bacteria). After 15-min incubation at 37 °C and 5 % CO_2, the moulds were removed obtaining hydrogel disks with 6 mm diameter and 2 mm thickness. Then, 4 mL of DMEM medium supplemented with 10 % FBS, 10 μg mL^{-1} tetracycline, 10 μg mL^{-1} chloramphenicol, 0.5 % NEAA and 2 mM L-glutamine was added to the wells containing the hydrogels. This media was referred to as DMEM-B and it was formulated in order to inhibit bacterial metabolism and control media acidification, since tetracycline is a bacterial RNA polymerase inhibitor that reduces the proliferation ratio of *L. lactis*, while chloramphenicol is used to maintain the plasmid that contains the BMP-2 gene in the bacteria [15]. The same protocol was followed to encapsulate hMSCs and *L. lactis* in non-mineralized Alg hydrogels (Alg + bacteria) by eliminating phosphate ions from the Alg solution.

Mineralized (Alg/HA) and non-mineralized (Alg) hydrogels encapsulating only hMSCs were synthesized as control living hydrogels by mixing in each hole 100 μL of Alg solution (with and without phosphate, respectively) containing 5 x 10^5 cells mL^{-1} with 50 μL of calcium chloride solution (0.2 M). After 15 min incubation at 37 °C and 5 % CO_2, the moulds were removed and 4 mL of the DMEM medium supplemented with 10 % FBS, 1 % NEAA, 1 % sodium pyruvate and 2 % antibiotics (6.74 U mL^{-1} penicillin-streptomycin, 0.2 μg mL^{-1} fungizone) and 2 mM L-glutamine was added. This media was referred to as DMEM-A. Three replicates of each living hydrogel (Alg, Alg/HA, Alg + bacteria, Alg/HA + bacteria) were used for each time point. Culture media was changed every 2–3 days.

After the cell culture, calcium could be chelated from the hydrogel and alginate chains recovered in solution. This should also allow the recovery of the HA nanocrystals and, ideally, the possibility of producing and re-use the hydrogels. However, this recycling process has not been evaluated in this work.

2.3.5. hMSC viability in the 3D hydrogels

To assess the viability of hMSCs cultured in living hydrogels for 1, 3 and 8 days the LIVE/DEAD® viability/cytotoxity kit (Molecular Probes, UK) was used. Briefly, the hydrogels were washed once with PBS at 37 °C and incubated for 30 min at 37 °C with 150 μL of a mixture containing 4 μM ethidium homodimer-1 and 2 μM calcein AM in PBS. Then, the staining solution was removed and the living hydrogels were washed with PBS. The distribution of live cells (green) and dead cells (red) in each hydrogel was visualized using an Axio Observer Z1 epifluorescence inverted microscope (Zeiss, GmbH, Germany). Cell viability was calculated by determining the ratio between live (green) and total number of cells (green plus red, live and dead cells) using ImageJ software (National Institutes of Health (NIH), USA).

2.4. Osteogenic differentiation of hMSCs

The potential of hybrid living hydrogels to induce osteogenic differentiation of hMSC was studied after 15 days. As described in the Section 2.3.4, hMSC embedded in Alg/HA and Alg/HA + Bacteria hydrogels were cultured in DMEM-A and DMEM-B media, respectively. For the positive control, hMSCs were encapsulated in mineralized hydrogel without bacteria and cultured in the DMEM-A media supplemented with 5 μg mL^{-1} BMP-2 (Alg/HA + BMP-2). hMSCs embedded in bacteria-containing hydrogels were cultured in DMEM-B media supplemented with 10 ng mL^{-1} of nisin to induce the expression of BMP-2 (Alg + Bacteria+Nisin and Alg/HA + Bacteria+Nisin) [5,15].

2.4.1. Gene expression of osteogenic markers

The osteogenic differentiation of hMSCs was evaluated by quantitative real-time polymerase chain reaction with reverse transcription (qRT-PCR).

After 15 days of cell culture, the living hydrogels were degraded in a solution containing 400 μL of 0.1 M sodium citrate and 10 μL of 2,2′,2″,2‴-(ethane-1,2 diyldinitrilo) tetraacetic acid (EDTA) mixing up and down with a pipette for 1 min. The supernatant was collected by centrifugation and total RNA from hMSCs was extracted and purified using a Rneasy Micro kit (Qiagen) following the manufacturer's instructions. The RNA concentration of each sample was measured using a spectrophotometer (Nanodrop 2000c, Thermo-Fisher Scientific, UK). The reverse transcription (cDNA) was performed using the QuantiTect Reverse Transcription Kit (Qiagen, Netherland). Forward and reverse primer sequences for qRT-PCR are listed in Table 2. Osteopontin (OPN) and osteocalcin (OCN) genes were selected due to their role in late osteogenic differentiation. Glyceraldehyde 3-phosphate dehydrogenase (GAPDH) was used as house-keeping gene to standardize gene expression levels. SYBR Green dye was used to target synthesized cDNA (Qiagen, Netherland). Then, qRT-PCR was carried out in a 7500 Fast Real Time PCR system (Applied Bio-system, USA) and the $2^{-\Delta\Delta Ct}$ method was performed for data analysis.

2.4.2. Osteogenic differentiation quantification by immunofluorescence

After 15 days of cell culture, hydrogels were washed with PBS twice and then fixed with a 4 % paraformaldehyde (PFA) solution in PBS at room temperature for 15 min. Fixative solution was removed and the samples were washed three times with PBS. Hereafter, cells were permeabilized with a solution of 0.1 % Triton X-100 in PBS for 5 min. To avoid non-specific binding, the samples were blocked by incubating in 2 % bovine serum albumin (BSA) in PBS for 30 min at 37 °C. After that, hydrogels were placed in a 96-well plate and incubated with anti-osteopontin rabbit primary polyclonal antibody (315,165,003, Jackson ImmunoResearch Laboratories Inc., USA) (1:150 in 2 % BSA in PBS) for 1 h at 37 °C. The samples were consequently washed to remove unbound primary antibody with 1 % Tween 20 in PBS three times for 5 min. Samples were then incubated with goat anti-rabbit secondary antibody (111165003, Jackson ImmunoResearch Laboratories Inc., USA) and phalloidin Alexa Fluor 488 (Thermofisher Scientific, U.K.) (1:200 and 1:100 in 2 % BSA in PBS, respectively) for 1 h at room temperature in the absence of light. Then, the samples were washed three times with 1 % Tween 20 in PBS for 5 min. hMSCs and L. *lactis* nuclei were stained with Vectashield-DAPI mounting medium (Vector Laboratories, USA). Samples were imaged in a LSM980 confocal microscope (Zeiss, GmbH, Germany).

2.5. Statistical analysis

Statistical comparisons were analysed with GraphPad Prism software (version 6.0) by using one-way ANOVA and Bonferroni's *post hoc* test. When *p*-values were lower than the standard significance value of 0.05, differences in the numerical results were considered statistically significant.

3. Results and discussion

3.1. Scaffolding: mineralized 3D alginate hydrogels

First, a mineralization protocol was designed to produce hybrid organic/inorganic 3D Alg hydrogels (Fig. 1). Sodium Alg was mixed

Table 2
Primer sequences used for qRT-PCR.

Gene	Primer direction	Primer sequence (3′-5′)	Tm (°C)	% GC
GAPDH	Forward	TCAAGGCTGAGAACGGGAA	51.1	52.63
	Reverse	TGGGTGGCAGTGATGGCA	52.6	61.11
OCN	Forward	CAGCGAGGTAGTGAAGAGACC	56.3	57.14
	Reverse	TCTGGAGTTTATTTGGGAGCAG	53.0	45.45
OPN	Forward	AGCTGGATGACCAGAGTGCT	53.8	55.00
	Reverse	TGAAATTCATGGCTGTGGAA	47.7	40.00

with a solution containing phosphate, carbonate and citrate, ions found in bone mineral [30,32,38,39]. The addition of Ca^{2+} ions caused the simultaneous Alg cross-linking and calcium phosphate mineralization. First, the experimental conditions to produce consistent 3D hydrogels that encapsulate cells (both MSC and bacteria) were determined (Table 1). Weak translucent hydrogels that were not able to self-support after vial inversion were obtained at Ca^{2+} concentrations below 40 mM (Fig. SI1). For this reason, these conditions were excluded. Consistent hydrogels were instead obtained at 40 mM Ca^{2+} (Fig. SI and inset of Fig. 2a). FTIR spectra of these hydrogels showed the characteristic phosphate vibrational bands of apatite (Fig. SI2), thereby confirming the successful mineralization of the hydrogels. A further inspection by TEM imaging confirmed that the inorganic phase was closely associated with the inorganic matrix, recapitulating bone (Fig. 2a) [30–32]. It is worth mentioning that we did not observe apatite nanocrystals precipitating out of the organic matrix. Apatite nanocrystals were indeed found to specifically interact with the Alg matrix, as observed in the corresponding chemical maps (Ca: magenta; P: green) obtained by EDS (Fig. 2b). SAED pattern displayed the hydroxyapatite reflections (002, 112 and 004), with no preferential orientation, in contrast to mineralized collagen fibrils of bone, in which apatite nanocrystals are specifically oriented with the *c*-axis parallel to the collagen fibber [20,40]. The effective mineralization was further confirmed macroscopically by XRPD (Fig. 2c). The pattern of the organic/inorganic hybrid showed broad bands of diffuse scattering associated to the organic matrix and broad peaks characteristic of poorly crystalline apatite (*i.e.*, 002 and 211 reflections, JCPDS 9-432) with similar structural features to those observed in bone apatite [30]. A further analysis of this mineralized hydrogel by SEM revealed rough surface with poorly defined porosity (Fig. SI3).

Bulk mechanical features of the organic/inorganic hydrogels were also studied by shear rheology. Viscoelastic properties of the hydrogels, dominated by the combination of the degree of crosslinking of the polymer, the inorganic nanocrystals and the high quantity of water inside the hydrogel, were analysed in the Linear Viscoelastic Region (LVE). The resulting storage (G') and loss (G") moduli for mineralized and non-mineralized hydrogels are shown in Fig. SI3. G' was higher than G" in this LVE region, thereby confirming the elastic gel-like behaviour of the samples [33].

The Young's modulus (*E*) was calculated from the shear modulus (*i.e.*, *G'* at the LVE region where it is frequency independent) using Eq. (1) (Section 2.2.4.). *E* values of mineralized and non-mineralized hydrogels

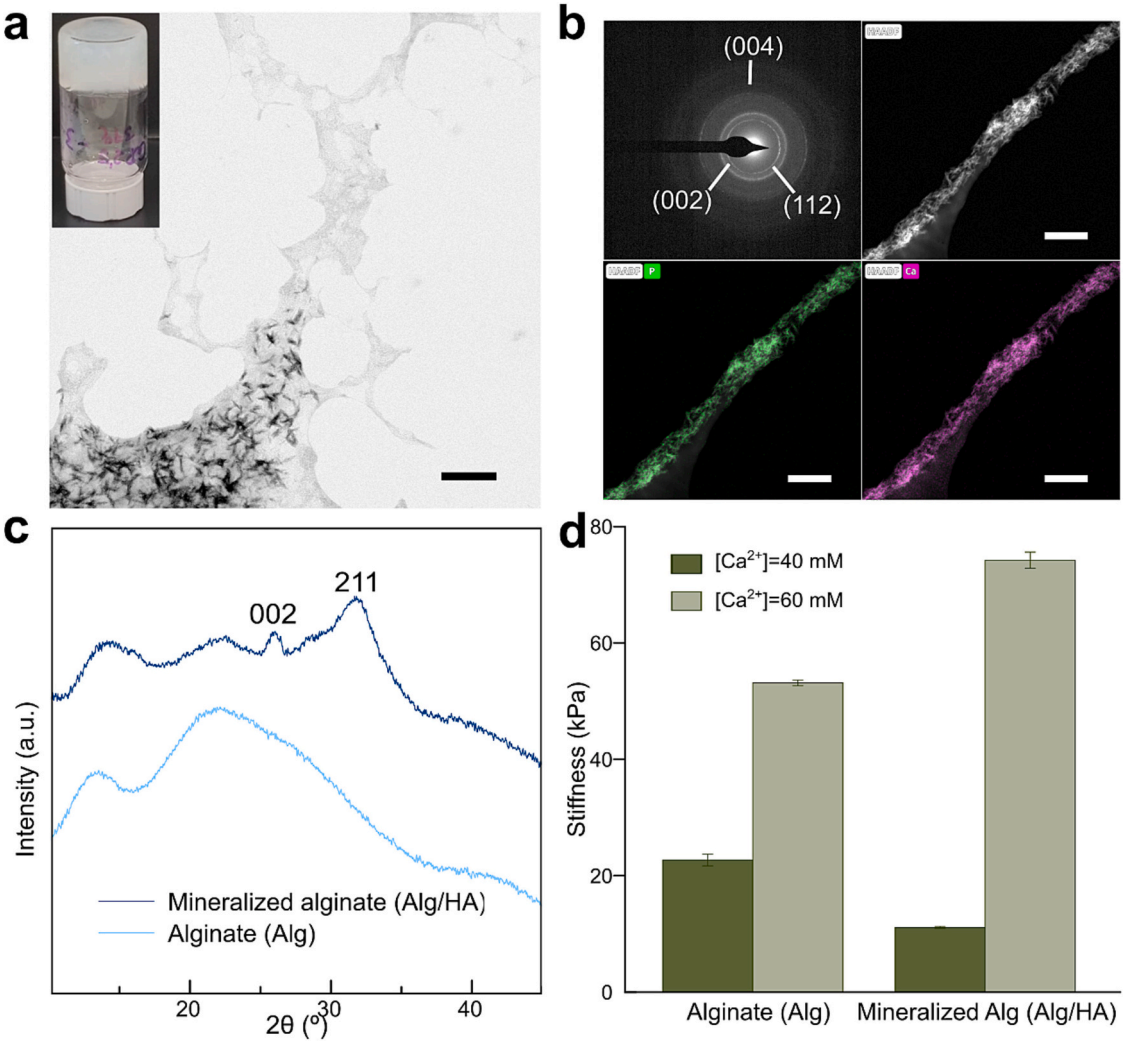

Fig. 2. Characterization of hybrid organic/inorganic hydrogels: a) TEM micrograph of mineralized alginate (Alg/HA) prepared at [Ca^{2+}] = 40 mM. Scale bar: 500 nm. Inset: inverted vial showing the consistency of the gel. b) SAED (up left), HAADF micrograph and corresponding EDS maps with P (green) and Ca (magenta) distributions demonstrating that calcium phosphate nanoparticles are formed in the Alg network. Scale bar: 500 nm. c) XRPD patterns of mineralized alginate (Alg/HA) and non-mineralized alginate as control (Alg). Main reflections of HA has been highlighted (according to JCPDS number 9-432). d) Young Moduli (*E*) represented as stiffness for mineralized (Alg/HA) and non-mineralized alginates (Alg) at two different Ca^{2+} concentrations after incubation at 37 °C for 24 h. Data show Means ± SD (n = 5).

are depicted in Fig. 2d. As described by the rubber elasticity theory, larger E values are achieved with higher number of crosslinks in the network [33,34], as a result of increasing Ca concentration. As mineralization is also calcium-consuming process, it did not lead to the expected proportional stiffening of the organic matrix ($E = 11.1 \pm 0.2$ kPa). This could be explained by the competition for calcium ions between Alg gelation and apatite nucleation, which would limit the crosslinking of Alg [29]. In fact, increasing the concentration of calcium ions from 40 mM to 60 mM resulted in much stiffer non-mineralized and mineralized hydrogels ($E = 74.2 \pm 1.4$ kPa). However, these latter hydrogels were opaque, hardly to be visualized through by confocal microscopy. Since alginate-based synthetic matrices with intermediate Young's moduli (between 11 and 30 kPa) are known to support the osteogenic differentiation of MSCs [41,42], we selected the transparent and soft hydrogels mineralized at 40 mM to support bacteria and hMSCs within living hydrogels.

3.2. Engineering living materials: introducing engineered bacteria and hMSCs in the mineralizing hydrogels

Engineered living materials were produced by integrating engineered *L. lactis* into the mineralized 3D matrix. The bottom-up synthetic approach used was the same shown in Fig. 1 but dispersing hMSCs and the engineered *L. lactis* in alginate solution prior to the addition of Ca^{2+} ions. Again, the addition of calcium ions ($[Ca^{2+}] = 40$ mM) prompted to the formation of a 3D matrix in which the living entities were entrapped (Fig. 3a). Both hMSCs viability and osteogenic differentiation resulting from the interaction with apatite nanoparticles and bacteria-released BMP-2 were evaluated.

hMSC viability in the presence and absence of HA and engineered *L. lactis* was assessed. Confocal laser scanning microscopy (CLSM) images of cells entrapped in Alg/HA, Alg/HA + bacteria, Alg and Alg + bacteria living hydrogels show a homogeneous distribution of live hMSCs in all the conditions (Fig. 3b) [39]. Cell viability in the different hydrogels did not display any statistical differences after 1 and 3 days, whereas after 8 days the Alg + bacteria hydrogel showed slightly higher viability compared to Alg/HA or Alg/HA + bacteria (Fig. 3c). Nonetheless, all the living hydrogels provided high cell viability values (>80 %) and are then well suited to be laden with mammalian cells.

3.3. hMSC osteogenic differentiation

The osteogenic differentiation of hMSCs laden in the living hydrogels was evaluated through the expression of osteocalcin (OCN) and osteopontin (OPN) at the gene and protein level. First, the gene expression of OCN and OPN was evaluated by qPCR after 15 days of culture (Fig. 4a–b). The important effect of BMP-2 in osteogenic differentiation of hMSCs has been widely described in the literature [43]. For this reason, this condition was used as positive control. Indeed, cells encapsulated within the positive control (Alg/HA gels treated with BMP-

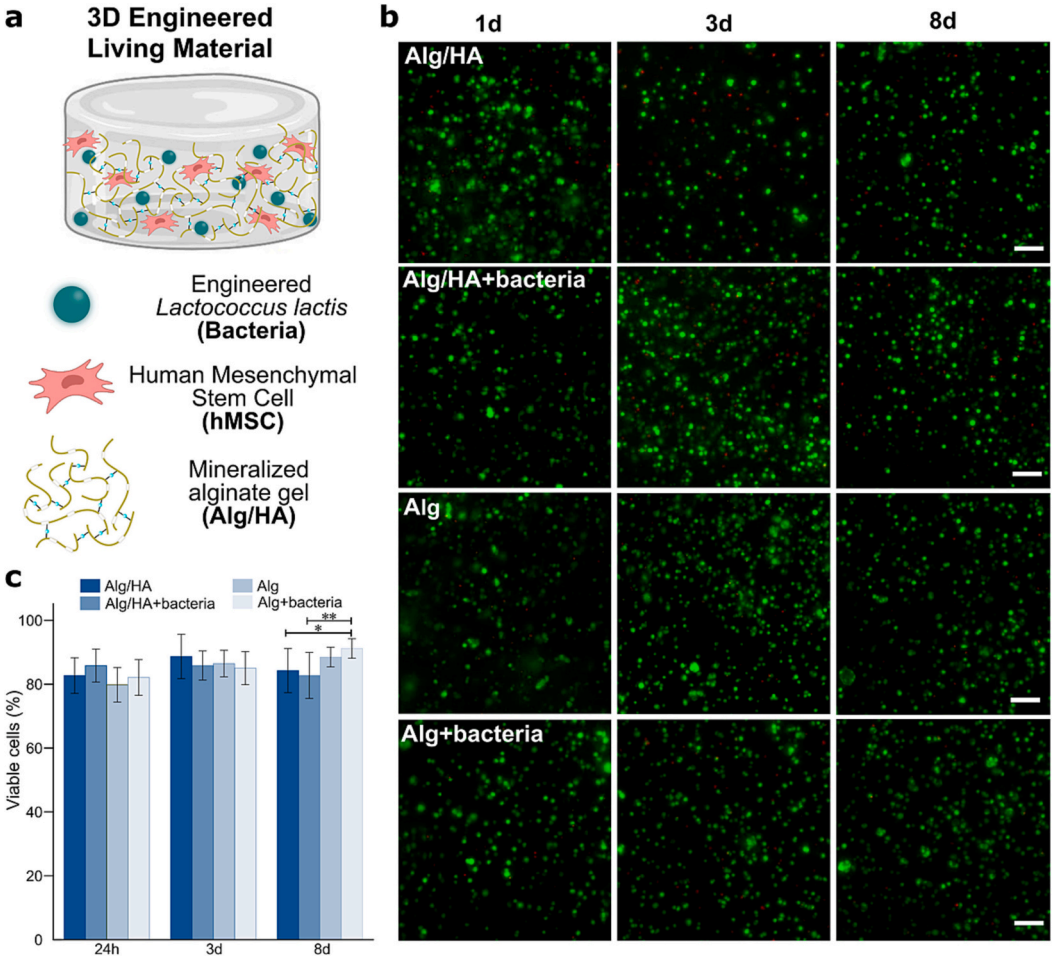

Fig. 3. Viability of hMSCs-laden living hydrogels a) Scheme of the proposed 3D engineered living material consisting of Alg/HA hydrogels, where the engineered *Lactococcus lactis* and hMSCs are encapsulated during the hydrogel formation and mineralization. b) Representative CLSM images showing the viability of hMSCs cultivated in Alg/HA, Alg/HA + Bacteria, Alg and Alg + bacteria hydrogels for 1, 3 and 8 days using a LIVE/DEAD® Viability/Cytotoxicity Kit. Live cells in green and dead cells in red. Scale bar: 200 μm. c) Cell viability in each hydrogel after 1, 3 and 8 days. The displayed data represent the mean ± SD (n = 6). * $p < 0.05$ and ** $p < 0.01$.

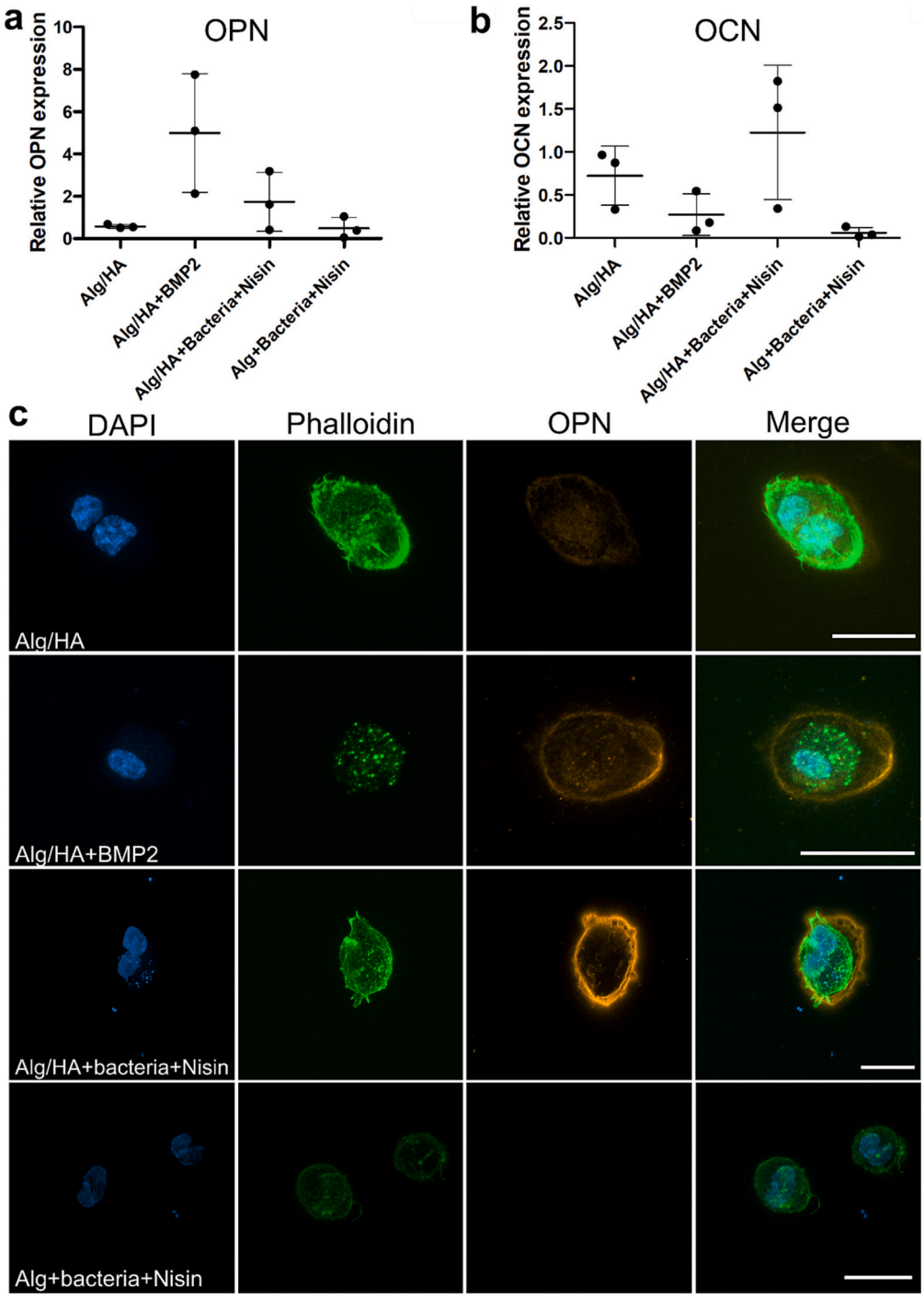

Fig. 4. hMSC were phenotyped using qRT-PCR to analyze gene expression of a) osteocalcin (OCN) and b) osteopontin (OPN). Cells were cultured for 15 days within the hydrogels and expression was normalized against GAPDH. c) Representative immunofluorescence images of hMSCs cultured for 15 days under different conditions. Images show nuclei (blue), actin cytoskeleton (green) and OPN (orange). Scale bar: 20 μm.

2) showed the highest mRNA expression of OPN (5-fold increase). The negative control consisted of encapsulated hMSCs within Alg/HA gels (without bacteria). Cells were still viable in the negative control (Fig. 3b–c), and as expected hMSCs did not undergo differentiation as demonstrated by the lack of OPN expression. Encapsulation of both engineered bacteria (inducible expression of BMP2 using 10 ng mL^{-1} of nisin [5]) and hMSCs within the Alg/HA gels resulted in a 2-fold increase in OPN but no enhanced expression of OCN which remains similar for all conditions including the positive control.

OPN expression was determined by immunostaining (Fig. 4c), with results aligned to the gene expression data previously discussed. OPN was visible in hMSCs encapsulated together with bacteria within Alg/HA gels and the positive control (Alg/HA gels +BMP2). It is interesting to note that HA is required to mediate the expression of OPN in the living hydrogels: engineered bacteria (induced with nisin) encapsulated with MSCs in Alg hydrogels did not lead to OPN expressions.

4. Conclusions

In this work, hybrid Alginate/HA hydrogels were synthesized, in-

depth characterized and then used to encapsulate hMSC and genetically engineered *L. lactis* (that express BMP2 upon nisin induction) to develop living hydrogels to induce osteogenic differentiation of hMSCs. Alginate gelation and mineralization occurred simultaneous resulting in stable and consistent hybrid hydrogels. The experimental conditions (*i.e.*, temperature, mineralization time and calcium concentration) were finely tuned to obtain hydrogels with stiffnesses that underping osteogenic differentiation of MSCs ($E = 11.1 \pm 0.2$ kPa). We demonstrated osteogenic differentiation of hMSC in the presence of the engineered bacteria and apatite after 15 days of culture, by both gene and protein expression. Mineralized Alg containing engineered bacteria produced an enhancement of OPN expression, relative to controls, demonstrating the synergistic effect between the engineered *L. lactis* and apatite to induce MSC differentiation.

CRediT authorship contribution statement

Belén Parra-Torrejón: Methodology, Investigation, Formal analysis, Visualization. **Vineetha Jayawarna:** Investigation, Formal analysis. **Aleixandre Rodrigo-Navarro:** Investigation, Formal analysis. **Juan Gonzalez-Valdivieso:** Investigation, Formal analysis. **Oana Dobre:** Investigation, Formal analysis. **Gloria B. Ramírez-Rodríguez:** Formal analysis, Supervision, Writing – original draft. **Manuel Salmeron-Sanchez:** Conceptualization, Supervision, Writing – original draft, Funding acquisition. **José M. Delgado-López:** Conceptualization, Supervision, Writing – original draft, Funding acquisition.

Declaration of competing interest

The authors declare that they have no known competing financial interests or personal relationships that could have appeared to influence the work reported in this paper.

Data availability

Data will be made available on request.

Acknowledgements

This study was supported by EPSRC (EP/P001114/1) and a grant from the U.K. Regenerative Medicine Platform "Acellular/Smart Materials-3D Architecture" (MR/R015651/1), Junta de Andalucía through the collaborative project NanoFERTI (P18-TP-0969) and the Spanish MCIN/AEI/10.13039/501100011033 and the "European Union" NextGenerationEU/PRTR (project number PDC2022-133191-I00). BPT and GBRR acknowledge the funding from the EMBO Scientific Exchange Grant (SEG number 9741) and RYC2021-032734-I funded by MCIN/AEI/10.13039/501100011033 and by "ESF Investing in your future", respectively.

Appendix A. Supplementary data

Supplementary data to this article can be found online at https://doi.org/10.1016/j.bioadv.2023.213587.

References

[1] G.L. Koons, M. Diba, A.G. Mikos, Materials design for bone-tissue engineering, Nat. Rev. Mater. 5 (2020) 584–603.
[2] H.J. Haugen, S.P. Lyngstadaas, F. Rossi, G. Perale, Bone grafts: which is the ideal biomaterial? J. Clin. Periodontol. 46 (2019) 92–102.
[3] A. Rodrigo-Navarro, S. Sankaran, M.J. Dalby, A. del Campo, M. Salmeron-Sanchez, Engineered living biomaterials, Nat. Rev. Mater. 6 (2021) 1175–1190.
[4] P.Q. Nguyen, N.M.D. Courchesne, A. Duraj-Thatte, P. Praveschotinunt, N.S. Joshi, Engineered living materials: prospects and challenges for using biological systems to direct the assembly of smart materials, Adv. Mater. 30 (2018) 1–34.
[5] J.J. Hay, A. Rodrigo-Navarro, M. Petaroudi, A.V. Bryksin, A.J. García, T.H. Barker, et al., Bacteria-based materials for stem cell engineering, Adv. Mater. 30 (2018) 1804310.
[6] C. Wang, Z. Zhang, J. Wang, Q. Wang, L. Shang, Biohybrid materials: structure design and biomedical applications, Mater. Today Bio 16 (2022), 100352.
[7] S. Yu, H. Sun, Y. Li, S. Wei, J. Xu, J. Liu, Hydrogels as promising platforms for engineered living bacteria-mediated therapeutic systems, Mater. Today Bio 16 (2022), 100435.
[8] L. Li, C. Yang, B. Ma, S. Lu, J. Liu, Y. Pan, et al., Hydrogel-encapsulated engineered microbial consortium as a photoautotrophic "living material" for promoting skin wound healing, ACS Appl. Mater. Interfaces 15 (2023) 6536–6547.
[9] Y. Lu, H. Li, J. Wang, M. Yao, Y. Peng, T. Liu, et al., Engineering bacteria-activated multifunctionalized hydrogel for promoting diabetic wound healing, Adv. Funct. Mater. 31 (2021) 2105749.
[10] C. Han, X. Zhang, G. Pang, Y. Zhang, H. Pan, L. Li, et al., Hydrogel microcapsules containing engineered bacteria for sustained production and release of protein drugs, Biomaterials 287 (2022), 121619.
[11] V. Hegde, U.T. Uthappa, T. Altalhi, H.Y. Jung, S.S. Han, M.D. Kurkuri, Alginate based polymeric systems for drug delivery, antibacterial/microbial, and wound dressing applications, Mater. Today Commun. 33 (2022), 104813.
[12] A.C. Hernández-González, L. Téllez-Jurado, L.M. Rodríguez-Lorenzo, Alginate hydrogels for bone tissue engineering, from injectables to bioprinting: a review, Carbohydr. Polym. 229 (2020), 115514.
[13] B.H.A. Rehm, M.F. Moradali, Alginates and Their Biomedical Applications 11, 2018.
[14] D.R. Sahoo, T. Biswal, Alginate and its application to tissue engineering, SN Appl. Sci. 3 (2021) 1–19.
[15] K. Witte, A. Rodrigo-Navarro, M. Salmeron-Sanchez, Bacteria-laden microgels as autonomous three-dimensional environments for stem cell engineering, Mater. Today Bio 2 (2019), 100011.
[16] M.M. Stevens, J.H. George, Exploring and engineering the cell surface interface, Science (80-) 310 (2005) 1135–1138.
[17] P. Fratzl, H.S. Gupta, E.P. Paschalis, P. Roschger, Structure and mechanical quality of the collagen-mineral nano-composite in bone, J. Mater. Chem. 14 (2004) 2115–2123.
[18] W. Landis, R. Jacquet, Association of calcium and phosphate ions with collagen in the mineralization of vertebrate tissues, Calcif. Tissue Int. 93 (2013) 329–337.
[19] M.J. Olszta, X. Cheng, S.S. Jee, R. Kumar, Y.-Y. Kim, M.J. Kaufman, et al., Bone structure and formation: a new perspective, Mater. Sci. Eng. R Reports 58 (2007) 77–116.
[20] F. Nudelman, N.A.J.M. Sommerdijk, Biomineralization as an inspiration for materials chemistry, Angew. Chem. Int. Ed. 51 (2012) 6582–6596.
[21] U.G.K. Wegst, H. Bai, E. Saiz, A.P. Tomsia, R.O. Ritchie, Bioinspired structural materials, Nat. Mater. 14 (2014) 23.
[22] G. Ramírez Rodríguez, T. Patrício, J.M. Delgado-López, Natural Polymers for Bone Repair, Second Edi, Elsevier Ltd, 2019.
[23] Z. Nie, Y. Zhang, R. Tang, X. Wang, Biomimetic mineralization: an emerging organism engineering strategy for biomedical applications, J. Inorg. Biochem. 232 (2022), 111815.
[24] J.M. Delgado-López, F. Bertolotti, J. Lyngsø, J.S. Pedersen, A. Cervellino, N. Masciocchi, et al., The synergic role of collagen and citrate in stabilizing amorphous calcium phosphate precursors with platy morphology, Acta Biomater. 49 (2017) 555–562.
[25] Y. Luo, Y. Li, X. Qin, Q. Wa, 3D printing of concentrated alginate/gelatin scaffolds with homogeneous nano apatite coating for bone tissue engineering, Mater. Des. 146 (2018) 12–19.
[26] S. Minardi, F. Taraballi, F.J. Cabrera, J. Van Eps, X. Wang, S.A. Gazze, et al., Biomimetic hydroxyapatite/collagen composite drives bone niche recapitulation in a rabbit orthotopic model, Mater. Today Bio 2 (2019), 100005.
[27] K. Liang, C. Zhao, C. Song, L. Zhao, P. Qiu, S. Wang, et al., In situ biomimetic mineralization of bone-like hydroxyapatite in hydrogel for the acceleration of bone regeneration, ACS Appl. Mater. Interfaces 15 (2023) 292–308.
[28] M.C. Echave, I. Erezuma, N. Golafshan, M. Castilho, F.B. Kadumudi, C. Pimenta-Lopes, et al., Bioinspired gelatin/bioceramic composites loaded with bone morphogenetic protein-2 (BMP-2) promote osteoporotic bone repair, Mater. Sci. Eng. C 134 (2021), 112539.
[29] M.C. Mañas-Torres, G.B. Ramírez-Rodríguez, J.I. García-Peiro, B. Parra-Torrejón, J. M. Cuerva, M.T. Lopez-Lopez, et al., Organic/inorganic hydrogels by simultaneous self-assembly and mineralization of aromatic short-peptides, Inorg. Chem. Front. 9 (2022) 743–752.
[30] J.M. Delgado-López, M. Iafisco, I. Rodríguez, A. Tampieri, M. Prat, J. Gómez-Morales, Crystallization of bioinspired citrate-functionalized nanoapatite with tailored carbonate content, Acta Biomater. 8 (2012) 3491–3499.
[31] J.M. Delgado-López, R. Frison, A. Cervellino, J. Gómez-Morales, A. Guagliardi, N. Masciocchi, Crystal size, morphology, and growth mechanism in bio-inspired apatite nanocrystals, Adv. Funct. Mater. 24 (2014) 1090–1099.
[32] Y.Y. Hu, A. Rawal, K. Schmidt-Rohr, Strongly bound citrate stabilizes the apatite nanocrystals in bone, Proc. Natl. Acad. Sci. U. S. A. 107 (2010) 22425–22429.
[33] A.M. Kloxin, C.J. Kloxin, C.N. Bowman, K.S. Anseth, Mechanical properties of cellularly responsive hydrogels and their experimental determination, Adv. Mater. 22 (2010) 3484–3494.
[34] O. Dobre, M.A.G. Oliva, G. Ciccone, S. Trujillo, A. Rodrigo-Navarro, D.C. Venters, et al., A hydrogel platform that incorporates laminin isoforms for efficient presentation of growth factors – neural growth and osteogenesis, Adv. Funct. Mater. 31 (2021).

[35] R.S. Bongers, M.H.N. Hoefnagel, M.J.C. Starrenburg, M.A.J. Siemerink, J.G. A. Arends, J. Hugenholtz, et al., IS981-mediated adaptive evolution recovers lactate production by ldhB transcription activation in a lactate dehydrogenase-deficient strain of Lactococcus lactis, J. Bacteriol. 185 (2003) 4499–4507.
[36] M. Petaroudi, A. Rodrigo-Navarro, O. Dobre, M.J. Dalby, M. Salmeron-Sanchez, Living biointerfaces for the maintenance of mesenchymal stem cell phenotypes, Adv. Funct. Mater. 32 (2022).
[37] M. Singh, D.A. Close, S. Mukundan, P.A. Johnston, S. Sant, Production of uniform, Assay Drug Dev. Technol. 13 (2015) 570–583.
[38] Y. Chen, W. Gu, H. Pan, S. Jiang, R. Tang, Stabilizing amorphous calcium phosphate phase by citrate adsorption, CrystEngComm 16 (2014) 1864–1867.
[39] N. Raja, H. Park, Y.J. Choi, H.S. Yun, Multifunctional calcium-deficient hydroxyl apatite-alginate core-shell-structured bone substitutes as cell and drug delivery vehicles for bone tissue regeneration, ACS Biomater. Sci. Eng. 7 (2021) 1123–1133.
[40] Y. Wang, T. Azais, M. Robin, A. Vallee, C. Catania, P. Legriel, et al., The predominant role of collagen in the nucleation, growth, structure and orientation of bone apatite, Nat. Mater. 11 (2012) 724–733.
[41] N. Huebsch, P.R. Arany, A.S. Mao, D. Shvartsman, O.A. Ali, S.A. Bencherif, et al., Harnessing traction-mediated manipulation of the cell/matrix interface to control stem-cell fate, Nat. Mater. 9 (2010) 518–526.
[42] X. Bai, M. Gao, S. Syed, J. Zhuang, X. Xu, X.Q. Zhang, Bioactive hydrogels for bone regeneration, Bioact. Mater. 3 (2018) 401–417.
[43] H. Cai, J. Zou, W. Wang, A. Yang, BMP2 induces hMSC osteogenesis and matrix remodeling, Mol. Med. Rep. 23 (2021) 1–12.